Robotic Assistant for Transperineal Prostate Interventions in 3T Closed MRI

Gregory S. Fischer[1], Simon P. DiMaio[2],
Iulian I. Iordachita[1], and Gabor Fichtinger[1]

[1] Center for Computer Integrated Surgery, Johns Hopkins University, USA
[gfischer,iordachita,gaborf]@jhu.edu,
[2] Surgical Planning Lab, Harvard University, USA
simond@bwh.harvard.edu.

Abstract. Numerous studies have demonstrated the efficacy of image-guided needle-based therapy and biopsy in the management of prostate cancer. The accuracy of traditional prostate interventions performed using transrectal ultrasound (TRUS) is limited by image fidelity, needle template guides, needle deflection and tissue deformation. Magnetic Resonance Imaging (MRI) is an ideal modality for guiding and monitoring such interventions due to its excellent visualization of the prostate, its sub-structure and surrounding tissues. We have designed a comprehensive robotic assistant system that allows prostate biopsy and brachytherapy procedures to be performed entirely inside a 3T closed MRI scanner. We present a detailed design of the robotic manipulator and an evaluation of its usability and MR compatibility.

1 Introduction

Core needle biopsy is considered the definitive method of diagnosis for prostate cancer, and each year approximately 1.5M core needle biopsies are performed, yielding about 220,000 new prostate cancer cases in the U.S. [1]. When cancer is confined to the prostate, low-dose-rate permanent brachytherapy, where 50-150 radioactive pellets/seeds are placed into the prostate, is a common treatment option. A complex seed distribution pattern must be achieved, while minimizing radiation toxicity to adjacent healthy tissues. Transrectal Ultrasound (TRUS) is the current "gold standard" for guiding biopsy and brachytherapy. However, current TRUS-guided biopsy has a detection rate of 20-30% [2] and TRUS-guided brachytherapy cannot readily visualize seed placement in the US images. Further, the template in TRUS-guided procedures limits the placement precision and the ability to effectively guide oblique insertions. MRI has high sensitivity for detecting prostate tumors, high spatial resolution, excellent soft tissue contrast and multiplanar volumetric imaging capabilities, making it an ideal modality for guiding and monitoring such procedures.

The clinical efficacy of MRI-guided prostate biopsy and brachytherapy was demonstrated by D'Amico, Tempany, et al. using a 0.5T open-MRI scanner to plan and monitor transperineal needle placement [3]. Needles were manually

N. Ayache, S. Ourselin, A. Maeder (Eds.): MICCAI 2007, Part I, LNCS 4791, pp. 425–433, 2007.

inserted using a plastic template, with the patient oriented in the lithotomy position, similarly to the TRUS-guided approach. Beyersdorff et al. performed targeted transrectal biopsy in 1.5T MRI with a passive articulated needle guide [4]. Krieger et al. present a 2-DOF passive, un-encoded and manually manipulated mechanical linkage to aim a needle guide for transrectal prostate biopsy with MRI guidance [5]. Robotic assistance has been investigated for guiding instrument placement in MRI, beginning with neurosurgery [6] and later percutaneous interventions [7]. Chinzei et al. developed a general-purpose robotic assistant for open MRI [8] that was subsequently adapted for transperineal intra-prostatic needle placement [9]. Stoianovici et al. has made developments in pneumatic stepper motors and applied them to robotic brachytherapy seed placement [10]. Other MRI-compatible mechanisms include pneumatic motors for a light puncture robot [11] and haptic interfaces for fMRI [12].

The patient is in the prone postion in [4] and [5], which make preoperative and intraoperative image fusion difficult; further, the transrectal approach precludes using commercially available endorectal imaging coils. The system presented in [10] is very complex and places the the patient in the fetal position, again preventing the pre- and intra-operative images from aligning and challenges traditional patient positioning for both MR imaging and and brachytherapy. The presented robotic system is of simpler design, lower cost, and above all, incorporates ergonomics suited for prostate biopsy and brachytherapy by allowing the patient to retain the supine (semi-lithotomy) pose used for preoperative imaging.

This work presents the design and development of a comprehensive robot-assisted system for transperineal prostate needle placement in 3T closed-bore MRI. The system integrates an image-based target planning interface, a robotic placement mechanism that allows for remote manipulation of the needle in the magnet bore without moving the patient out of the imaging space, as well as robot and needle tracking for navigation and control.

2 Methods

2.1 System Layout and Architecture

We have developed a comprehensive computer-integrated needle placement system to accurately target planned tissue sites by minimizing needle misplacement effects. The complete system comprises two main modules, integrated with high-field diagnostic MRI scanners. First is a visualization, planning and navigation system, and second is a robotic assistant for needle placement. The architecture of this system is outlined in Fig. 1.

In blocks **a** and **b**, 3D Slicer software (www.slicer.org) fuses multimodality pre-operative images with pre-procedural MR images for procedure planning. Kinematics of the needle trajectories are evaluated subject to anatomical constraints and constraints of the needle placement mechanism. Device and needle navigation are shown in blocks **c**, **d** and **e**, which are enclosed in a loop that represents device/needle positioning and sensing/localization. Blocks **d** and **e** guide the needle positioning device; an image-based servo loop tracks the needle

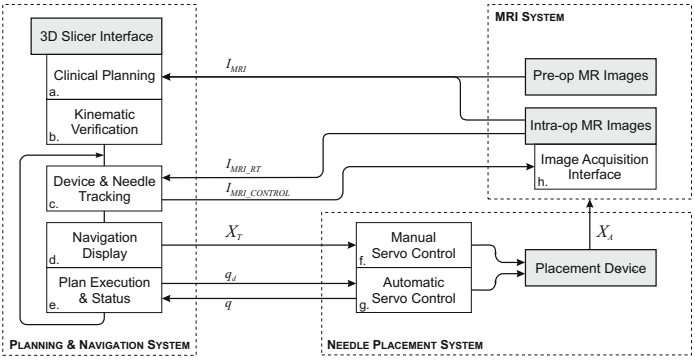

Fig. 1. System architecture (left) and component distribution (right)

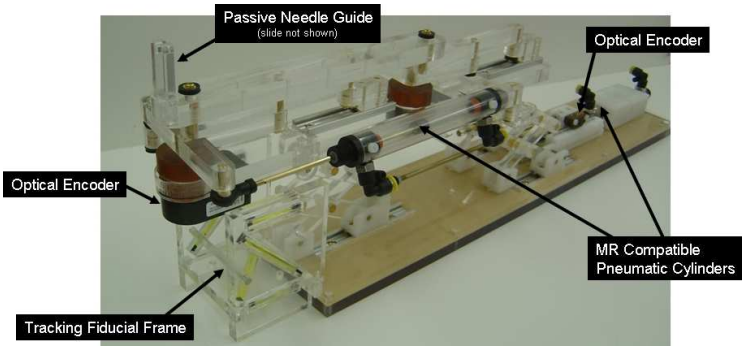

Fig. 2. Robot manipulator capable of two actuated DOFs with manual needle insertion. The tracking fiducial frame at the front of the robot is used for locating the robot in the scanner coordinate system.

and provides real-time images along it's axis to help detect and limit needle and tissue deflection effects. Blocks **f** and **g** are the robotic mechanism that provides remote operation of the needle while the patient is within the magnet bore.

2.2 Mechanical Design

The patient is positioned in the supine position such that their legs are placed on a leg support that provides a "tunnel" of access to the perineum. This creates a well defined workspace at the patient's perineum, while maintaining a compact profile to prevent interference with the patient, the scanner and adjacent equipment. The focus of the first phase is to bring MR guidance to the same degrees of freedom (DOF) available in traditional TRUS template-guided procedures. The kinematic requirements are $100mm$ in the vertical and horizontal directions and passive needle insertion guide with an encoded travel of $120mm$. To mimic the traditional TRUS procedure and also for increased safety, needle insertion

is performed manually along the needle guide that is aligned by the robot. Already incorporated in the mechanical design, but not actuated in the present prototype system are two additional DOF; 15° of rotation in the vertical and horizontal planes will help avoid pubic arch interference that may typically be a contraindication using traditional techniques. This will be particularly important since space constraints of the MR scanner prevent positioning the patient in the full lithotomy position; thus, lowering the pubic arch and increasing the likelyhood of interference.

Vertical motion is generated by a modified scissor lift mechanism. Two such mechanisms actuated independently provide vertical motion and elevation angle. Horizontal motion is generated by a second planar bar mechanism that rests upon the vertical stage. Prismatic and rotational motions can be realized by coupling two such straight-line motion mechanisms. For both stages, actuation is provided by custom pneumatic cylinders described in Section 2.3. The actuators are oriented along the bore axis (B_0), thus reducing the overall width significantly. The complete assembly is shown in Fig. 2. Sterility is insured by making the top-most portion of the passive needle guide removable and draping the remainder of the robot. Further, the tissue contacting surface of the leg rest will be removable and sterilizable.

2.3 Actuation and Control

Pneumatic actuators were chosen because they offer relatively high speed and power for their weight and provide for compact means of actuation at the mechanism. They also do not require involved setup or allow the risk of fluid leakage, which is a sterility concern, associated with hydraulic systems. Servo control of the cylinders is provided by piezoelectrically actuated pressure regulator valves with switching times under $4ms$ (Hoerbiger-Origa Tecno Valve, Altenstadt, Germany). Custom MR compatible pneumatic cylinders are made with glass bores, graphite pistons, brass shafts and plastic housings (Made in collaboration with Airpel, Norwalk, CT). Pneumatic brakes are attached to each cylinder in order to lock and maintain needle position/orientation during needle insertion. They are unlocked by applying air pressure.

The robot uses linear strip optical encoders for the vertical motion stage and rotary encoders on the horizontal motion stage. Encoders were thoroughly tested in 3T MRI for functionality and imaging compatibility (US Digital EM1 with PC5 differential driver, Vancouver, Washington). Functionality was evaluated by confirming that no encoder counts were lost as the mechanism periodically oscillated in the bore of the scanner during imaging. Imaging compatibility was confirmed by monitoring the effect on the MR images under standard prostate imaging protocols as described later in Section 3.1.

A controller sitting in the MR scanner room near the foot of the bed provides low level control of the robot. Inside of the EMI shielded enclosure is an embedded computer with analog I/O for interfacing with valves and pressure sensors and an FPGA module for interfacing with joint encoders. Also in the enclosure are piezoelectric servo valves, piezoelectric brake valves and pressure

sensors. The short distance between the servo valves and the robot is minimized, thus maximizing the bandwidth of the pneumatic actuators. The expected bandwidth is 100Hz. Control software on the embedded PC provides for low-level joint control and an interface to interactive scripting and higher-level trajectory planning. Communication with the planning and control workstation is through a fiberoptic ethernet connection.

Dynamic global registration between the robot and scanner is provided by passive tracking fiducials on the robot base and is described in detail in [13]. The rigid structure of the the fiducial frame is made up of seven rigid glass tubes with $3mm$ inner diameters that are filled with contrast extracted from MR Spot fiducials (Beekley, Bristol, CT). The rods are placed on three faces of a $60mm$ cube as shown in Fig. 2, and any arbitrary MR image slicing through all of the rods provides the full 6 DOF pose of the frame, and thus the robot, with respect to the scanner. Thus, by locating the fiducial attached to the robot, the transformation between patient coordinates (where planning is performed) and the robot's needle driver is known.

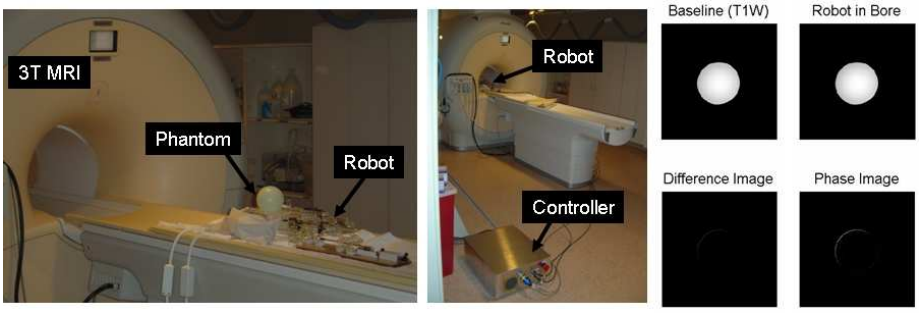

Fig. 3. Experimental setup for compatibility trials. The robot is placed on the bed alongside a spherical MR phantom (left) and the controller is placed in the scanner room near the foot of the bed(center). Images of the spherical phantom taken with the T1W sequence are shown with and without the robot present; the square at the center represents the field of view used for SNR calculations. Below them are the corresponding difference and phase images (right).

3 Results

3.1 MR Compatibility

MR Compatibility includes three main elements: 1) safety, 2) preserving image quality, and 3) maintaining functionality. Safety issues such as RF heating are minimized by isolating the robot from the patient, avoiding wire coils, and avoiding resonances in components of the robot; ferrous materials are completely avoided to prevent the chance of a projectile. Image quality is maintained by again avoiding ferromagnetic materials, limiting conductive materials near the

imaging site, and avoiding RF sources. Pneumatic actuation and optical sensing, as described in Section 2.3, preserve full functionality of the robot in the scanner.

Evaluation and verification of the MR compatibility of the system was a primary goal of this work. Compatibility was evaluated on a 3T Philips Achieva scanner. A 10cm spherical MR phantom was placed at the isocenter and the robot placed such that the tip was at a distance of 120mm from the center of the phantom (a realistic depth from perineum to prostate) as shown in Fig. 3 (left). The phantom was imaged using three standard prostate imaging protocols: 1) **T2W TSE**: T2 weighted turbo spin echo (28cm FOV, 3mm slice, TE=90ms, TR=5600ms, 2) **T1W FFE**: T1 weighted fast field gradient echo (28cm FOV, 3mm slice, TE=2.3ms, TR=264ms) and 3) **TFE (FGRE)**: "Real time" turbo field gradient echo (28cm FOV, 3mm slice, TE=10ms, TR=26ms). A baseline scan with each sequence was taken of the phantom with no robot components using round flex coils similar to those often used in prostate imaging. The following imaging series were taken in each of the following configurations: 1) Phantom only, 2) Controller in room and powered, 3) Robot placed in scanner bore, 4) Robot electrically connected to controller and 5) Robot moving during imaging (only with T1W imaging). For each step, all three imaging sequences were performed and both magnitude and phase images were collected.

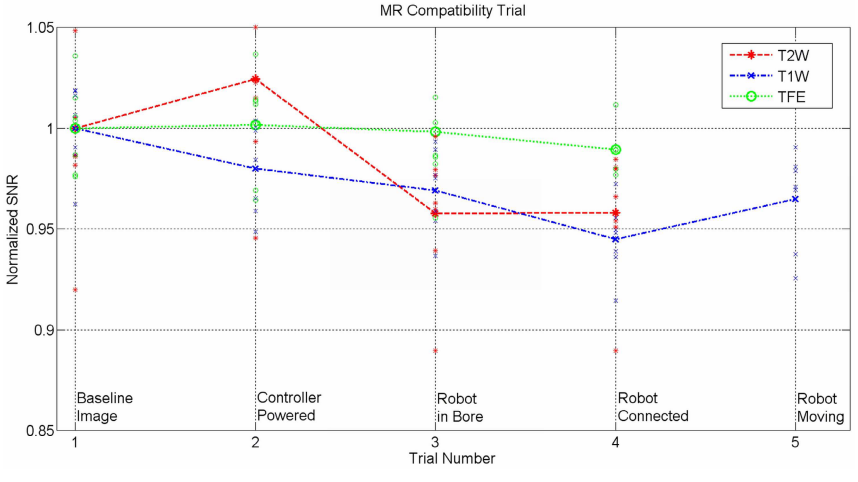

Fig. 4. Signal to noise ratio for three standard prostate imaging protocols with the system in different configurations. Lines represent mean SNR within 25mm cube at center of homogeneous phantom and discrete points represent SNR in the 25mm square on each of seven 3mm slices making up the cube.

The effect on image quality was judged by computing the signal to noise ratio (SNR). SNR of an MR image can be calculated with several techniques; we chose to define it as the mean signal in a 25mm square at the center of the homogeneous sphere divided by the standard deviation of the signal in that same region as shown in Fig. 3 (right). The SNR of the magnitude images was normalized by

the value for the baseline image, thus limiting any bias in choice of calculation technique or location. SNR was evaluated at seven slices (representing 25mm width) at the center of the sphere for each of the three imaging sequences. The points in the graph in Fig. 4 show the SNR in the phantom for seven $3mm$ thick slices for each sequence at each configuration. The lines represent the average SNR in the $25mm$ cube at the center of the spherical phantom for each sequence at each configuration. When the robot was operational, the reduction in SNR of the $25mm$ cube at the phantom's center for these pulse sequences was 5.5% for **T1W FFE**, 4.2% for **T2W TSE** and 1.1% for **TFE (FGRE)**. Further qualitative means of evaluating the effect of the robot on image quality are obtained by examining prostate images taken both with and without the robot present. Fig. 5 (right) shows images of the prostate of a volunteer placed in the scanner bore on the leg rest.

3.2 System Integration

To evaluate the overall layout and workflow, the robot was placed in the bore inside of the leg rest with a volunteer as shown in Fig. 5 (left). Round flex receiver coils were used for this trial; endorectal coils can be used for clinical case to obtain optimal image quality. There was adequate room for a patient and the robot was able to maintain its necessary workspace.

Co-registration of the robot to the scanner was performed using the base tracking fiducial described in Section 2.3 that is shown in Fig. 2. Images of the robot's tracking fiducial provide the location of the robot base in the scanner's coordinate system with an RMS accuracy of $0.14mm$ and 0.37^o as described in [13]. Joint encoding provides end effector localization resolution of better that $0.01mm$ and $0.1mm$ for horizontal and vertical motions, respectively. In free space, the needle tip localization accuracy with respect to the MR images is expected to be better than $0.25mm$ and 0.5^o.

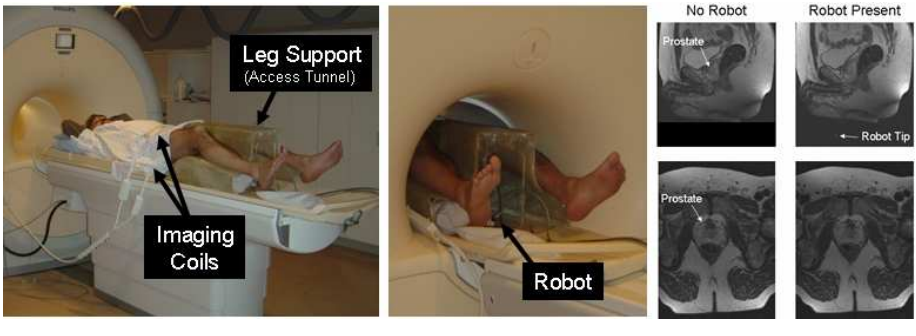

Fig. 5. Qualitative analysis of prostate image quality. Patient is placed on the leg support (left) and the robot sits inside of the support tunnel inside the scanner bore (center). T2 weighted sagittal and transverse images of the prostate taken when no robot components were present and when the robot was active in the scanner (right).

4 Discussion

MRI-guidance promises high quality, rapid, volumetric, multimodality imaging capabilities, but presents significant engineering challenges due to the harsh electromagnetic environment and tight spatial constraints in the scanner bore. We have developed a prototype robotic system for precisely targeting prostate tissue under realtime MR guidance. The current system provides the 2-DOF plus insertion of traditional TRUS-guided procedures with finer spatial resolution and image-based guidance. Needle placement accuracy can be improved from the $5mm$ grid that is standard today.

We have shown the system to be MR compatible under standard prostate imaging sequences, with sufficient accuracy for guiding prostate biopsy and brachytherapy procedures. Localization accuracy of the tracking fiducial that is attached to the robot and its application to visual servoing and dynamic scan plane control are described in our companion paper [13]. Detailed analysis of the true needle insertion error of the complete system in phantom studies, and ultimately animal and cadaver trials, is forthcoming. The next generation system will incorporate additional rotational DOFs such that pubic arch interference can be avoided, thus increasing the eligible population for these procedures. This work is also of relevance to the development of systems specialized for other organ systems and diseases that require targeted needle placement inside an MRI scanner.

This work was supported by NIH 1R01CA111288, CDMRP PCRP Fellowship W81XWH-07-1-0171, and NSF EEC-9731748.

References

1. Jemal, A., Siegel, R., Ward, E., Murray, T., Xu, J., Smigal, C., Thun, M.: Cancer statistics, 2006. CA Cancer J. Clin. 56(2), 106–130 (2004)
2. Terris, M.K., et al.: Comparison of mid-lobe versus lateral systematic sextant biopsies in detection of prostate cancer. Urol Int. 59, 239–242 (1997)
3. D'Amico, A.V., Tempany, C.M., Cormack, R., Hata, N., et al.: Transperineal magnetic resonance image guided prostate biopsy. J. Urol. 164(2), 385–387 (2000)
4. Beyersdorff, D., Winkel, A., Hamm, B., et al.: MRI-guided prostate biopsy with a closed MR unit at 1.5 T. Radiology 234, 576–581 (2005)
5. Krieger, A., Susil, R.C., Menard, C., Coleman, J.A., Fichtinger, G., Atalar, E., Whitcomb, L.L.: Design of a novel MRI compatible manipulator for image guided prostate interventions. IEEE TBME 52, 306–313 (2005)
6. Masamune, K., Kobayashi, E., Masutani, Y., Suzuki, M., Dohi, T., Iseki, H., Takakura, K.: Development of an MRI-compatible needle insertion manipulator for stereotactic neurosurgery. J. Image Guid. Surg. 1(4), 242–248 (1995)
7. Hempel, E., Fischer, H., Gumb, L., et al.: An MRI-compatible surgical robot for precise radiological interventions. In: CAS, pp. 180–191 (2003)
8. Chinzei, K., Hata, N., Jolesz, F.A., Kikinis, R.: MR compatible surgical assist robot: system integration and preliminary feasibility study. In: Delp, S.L., DiGoia, A.M., Jaramaz, B. (eds.) MICCAI 2000. LNCS, vol. 1935, pp. 921–933. Springer, Heidelberg (2000)

9. DiMaio, S.P., Pieper, S., Chinzei, K., Fichtinger, G., Tempany, C., Kikinis, R.: Robot assisted percutaneous intervention in open-MRI. In: MRI Symp. p. 155 (2004)
10. Muntener, M., Patriciu, A., Petrisor, D., Mazilu, D., Bagga, H., Kavoussi, L., Cleary, K., Stoianovici, D.: MRI compatible robotic system for fully automated brachytherapy seed placement. J. Urology 68, 1313–1317 (2006)
11. Taillant, E., Avila-Vilchis, J., Allegrini, C., Bricault, I., Cinquin, P.: CT and MR Compatible Light Puncture Robot: Architectural Design and First Experiments. In: Barillot, C., Haynor, D.R., Hellier, P. (eds.) MICCAI 2004. LNCS, vol. 3217, pp. 145–152. Springer, Heidelberg (2004)
12. Gassert, R., Moser, R., Burdet, E., Bleuler, H.: MRI/fMRI-Compatible Robotic System With Force Feedback for Interaction With Human Motion. T. Mech. 11(2), 216–224 (2006)
13. DiMaio, S., Samset, E., Fischer, G., Iordachita, I., Fichtinger, G., Jolesz, F., Tempany, C.: Dynamic MRI Scan Plane Control for Passive Tracking of Instruments and Devices. In: Ayache, N., Ourselin, S., Maeder, A. (eds.) MICCAI 2007. LNCS, vol. 4792, pp. 50–58. Springer, Heidelberg (2007)